



**HAL**  
open science

# Different physics but similar dependence of runout distance with discharge rate: the duality of pyroclastic density currents

Olivier Roche, Nourddine Azzaoui, Arnaud Guillin

## ► To cite this version:

Olivier Roche, Nourddine Azzaoui, Arnaud Guillin. Different physics but similar dependence of runout distance with discharge rate: the duality of pyroclastic density currents. *Bulletin of Volcanology*, 2024, 86 (7), pp.65. 10.1007/s00445-024-01750-8 . hal-04630062

**HAL Id: hal-04630062**

**<https://uca.hal.science/hal-04630062v1>**

Submitted on 1 Jul 2024

**HAL** is a multi-disciplinary open access archive for the deposit and dissemination of scientific research documents, whether they are published or not. The documents may come from teaching and research institutions in France or abroad, or from public or private research centers.

L'archive ouverte pluridisciplinaire **HAL**, est destinée au dépôt et à la diffusion de documents scientifiques de niveau recherche, publiés ou non, émanant des établissements d'enseignement et de recherche français ou étrangers, des laboratoires publics ou privés.



Distributed under a Creative Commons Attribution 4.0 International License

# Different physics but similar dependence of runout distance with discharge rate: the duality of pyroclastic density currents

Olivier Roche<sup>1\*</sup>, Nourddine Azzaoui<sup>2</sup>, Arnaud Guillin<sup>2</sup>

<sup>1</sup> Université Clermont Auvergne, CNRS, IRD, OPGC, Laboratoire Magmas et Volcans, F-63000 Clermont-Ferrand, France.

<sup>2</sup> Université Clermont Auvergne, CNRS, Laboratoire de Mathématiques Blaise Pascal, F-63000 Clermont-Ferrand, France.

\* Corresponding author (olivier.roche@uca.fr)

ORCID

OR: 0000-0002-6751-6904, NA: 0000-0002-1543-5440, AG: 0000-0003-2393-6242

## Abstract

We address emplacement mechanisms of pyroclastic density currents (PDCs) through relationships between their runout distance and mass discharge rate of their parent eruptions. Assuming axisymmetric propagation typical of dilute currents that are little controlled by topography, we apply a simple method to estimate the runout distance of concentrated PDCs channelized in valleys. With these data the runout distance of concentrated currents varies, as for their dilute counterparts, with the discharge rate to the power  $\sim 0.5$ , the latter being the consequence of radial propagation of the currents. This simple dependence between runout distance and discharge rate is both surprising and remarkable considering the fundamentally different natures of dilute or concentrated PDCs, which are governed by complex physics involving many parameters. This dependence further suggests that particle settling velocity, which controls the rate of decrease of the flow mass, has a second-order effect on the runout distance. We argue that the hindered settling model established for particle suspensions in a static fluid is relevant for estimating the settling velocity of particles in concentrated PDCs. Settling velocities of  $\sim 0.1$ -10 cm/s calculated for some natural examples correspond to deposit aggradation rates of same order. These rates imply timescales of deposit formation significantly shorter than flow durations in some cases, suggesting that onset of deposition occurs at late stages of emplacement.

## Keywords

Pyroclastic density currents, discharge rate, runout distance, power law relationship, particle hindered settling, deposit aggradation

## 1. Introduction

Complex physics control emplacement of pyroclastic density currents (PDCs) due to the multiphase nature of these mixtures, ranges of particle concentrations and related gas-particle and particle-particle interactions. In this regard, a better understanding of particle transport and deposition mechanisms is essential for establishing models of PDC emplacement to predict inundated areas in context of volcanic hazard assessment (e.g., Kelfoun et al. 2009; Charbonnier et al. 2013; Ogburn and Calder 2017; de' Michieli Vitturi et al. 2019; Esposti Ongaro et al. 2020; Gueugneau et al. 2021; Tadini et al. 2021; Aravena et al. 2020; Bevilacqua et al. 2022). The particle concentration in PDCs has long been thought to increase vertically downward and vary over several orders of magnitude (e.g., Fisher 1979; Valentine 1987; Ort et al. 2003; Druitt 1998), causing distinct particle transport mechanisms at different levels in the flows (Dufek 2016; Kelfoun 2017; Lube et al. 2020; Charbonnier et al. 2023). Many studies from the physics and engineering communities show that turbulent gas-particle mixtures are commonly heterogenous and that at bulk concentrations as low as 0.01-1 vol.% interparticle collisions and fluid drag related effects cause the formation of clusters of particles, which are regions of higher concentrations (Chen et al. 2016, Gustavsson and Mehlig 2016; Brandt and Coletti 2022). At larger bulk concentrations, the turbulence and the ability of the gas to transport solid particles are significantly damped. The densest mixtures with concentrations of  $\sim 40$ -50 vol.% are granular flows whose physics is controlled by particles interactions (Ort, 1993;

Sulpizio et al. 2016) and within which pore fluid pressure can be generated if the drag of the interstitial gas on the particles is high enough (Roche et al. 2010; Lube et al. 2019).

The present study addresses in particular PDCs generated by eruptive fountain collapse. Recent advances have shown that two types of PDCs can arise in the impact zone of a fountain depending on the eruptive conditions and the particle transport mechanisms described above (Sweeney and Valentine 2017; Valentine 2020) (Fig. 1). Collapsing pyroclastic mixtures that contain particles at concentrations  $< \sim 1$  vol.% and well-coupled to the gas remain dilute and turbulent upon impact. A PDC formed in this manner is characterized by a suspended load with clusters (Brosch and Lube 2020), above a bedload that results from the interaction of the current with the substrate (Dufek and Bergantz 2007; Andrews and Manga 2012; Douillet et al. 2013; Dellino et al. 2021). In contrast, mixtures that are more concentrated in particles and/or composed of a majority of particles poorly coupled to the gas accumulate in the impact zone to form a concentrated basal flow (Penlou et al. 2023b) overridden by a dilute suspension in which clusters emerge and feed the underlying flow (Breard et al. 2016), hence forming a two-layer current (Doyle et al. 2011; Shimizu et al. 2019, 2023). For convenience we use hereafter the terms *dilute* or *concentrated* to designate the currents described above.

Though dilute and concentrated PDCs are fundamentally different in nature, they share the same principle of progressive mass loss by settling of particles that accumulate to form an aggrading deposit (Fig. 1; Branney and Kokelaar 2002; Doronzo and Dellino 2013), except for dilute hot buoyant parts that lift off (Andrews 2014; Benage et al. 2016) or when basal flow conditions cause transient erosion of the deposit (Brown and Branney 2004; LaBerge et al. 2006; Fauria et al. 2016). In this context, the runout distance of a PDC is set as the flowing mixture runs out of mass and therefore it depends primarily on the balance between particle advection and particle settling (Dade and Huppert 1995). The particle settling velocity in dilute suspensions can be estimated from well-established theoretical laws (e.g., Dellino et al. 2008) but the formation of clusters can promote an intermediate flow regime (cf. Lube et al. 2020) and cause settling velocities that are significantly different than that of individual particles (Breard et al. 2016, Penlou et al. 2023a). In contrast, the particle settling velocity in concentrated flows, which controls the aggradation rate of the so-called static-mobile interface (or flow-boundary zone), remains poorly understood (Delannay et al. 2017; Trinh et al. 2017).

The objective of the present contribution is to discuss the runout of PDCs, with a specific focus on concentrated currents for which we provide estimates of particle settling velocities. In order for the reader to appreciate the context of our study, we first present recent work on factors that control runout of PDCs.

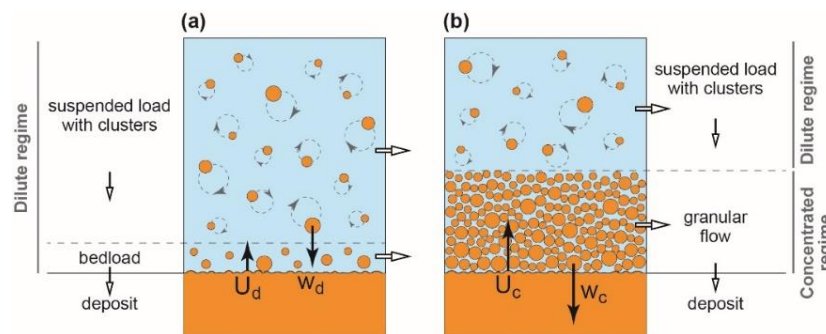


**Fig. 1.** Schematic representation of particle transport and deposition mechanisms in (a) dilute and (b) concentrated pyroclastic density currents. Horizontal and vertical white arrows indicate respectively flow direction and mass transfers in the stratified currents. Particles settle at typical velocity  $w$  and accumulate to form a deposit whose surface aggrades at velocity  $U$ .

## 2. Earlier works on runout distance of pyroclastic density currents

We summarize the study of Roche et al. (2021) whose statistical analysis shows that the eruption mass discharge rate is the main control parameter on the runout distance of PDCs (Fig. 2). In the framework defined by these authors, the mass discharge rate and the runout distance for a given eruption are mean values determined from published works respectively for the pyroclastic fountain phase (caused by partial to complete collapse of an eruptive column) and from the extent of PDC deposits in several directions from the vent(s). The mass discharge rate of the PDC phase is in most cases inferred from the discharge rate of the initial Plinian phase, which is calculated from plume height determined from isopleths of fall deposits. From data of well-documented eruptions for which estimates for both eruption phases are available, Roche et al. (2021, their Fig. 2) found that the discharge rate of the PDC phase is on average 13.6 times higher than that of the Plinian phase. This increase in discharge rate during eruptions is consistent with column collapse and onset of PDC generation, and it can be explained by conduit widening and opening of ring-fractures at onset of caldera collapse. Note that a decrease in volatile content in magmas also favors column collapse (Carazzo et al. 2008).

For dilute currents, the runout distance is

$$R_d = 11 \times 10^{-4} Q^{0.468}, \quad (1)$$

with  $Q$  the mass discharge rate (Fig. 2), and considering a typical particle settling velocity deduced from the mean particle size,  $w_d$ , then

$$R_d = 12 \times 10^{-4} (Q/w_d)^{0.484}. \quad (2)$$

The power law relationships given above are very close. This can be explained by the fact that  $Q$  varies over five orders of magnitude and is the main control parameter on the runout distance while  $w_d$  varies at most by a factor  $\sim 5$  and has a second order effect. Interestingly, Eq. (2) is in agreement with the findings of Dade and Huppert (1995) who showed that the runout of axisymmetric dilute turbulent particle-laden flows depends on the balance between advection and settling of particles, so that  $R_d$  scales with  $(Q'/w_d)^{0.5}$ , with  $Q'$  the volumetric flow rate. Assuming a constant magma density  $\rho = Q'/Q$  in the context of PDCs,  $R_d$  scales also with  $(Q/w_d)^{0.5}$ . Therefore, Eq. (2) suggests that the emplacement of dilute PDCs, which propagate radially with little influence of topography, obeys the principle defined by Dade and Huppert (1995).

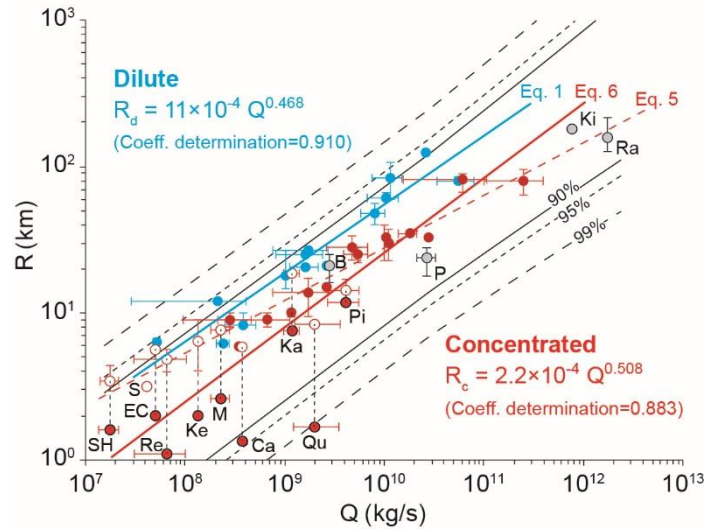


**Fig. 2.** Power law relationships between runout distance of dilute or concentrated PDCs,  $R$ , and mass discharge rate of parent eruptions,  $Q$ . The best fit line for dilute currents is given by Eq. (1) (blue line). For concentrated currents, the dashed red line is the best fit given by Eq. (5) for raw data of runout distance represented by red and white dots. Red dots with black contours stand for recalculated runout data for channelized currents (see text for explanation) and they are considered with raw data (red dots) to determine the best fit red line given by Eq. (6) and the associated 90-99% prediction intervals shown by black (dashed) lines. Recalculated runouts are those of the following eruptions: Ca (Calbuco), EC (El Chichon), Ka (Katmai), Ke (Kelud), M (Mount St Helens), Pi (Pinatubo), Qu (Quizapu), Re (Reventador), SH (Soufrière Hills), S (Spurr). The data for Quizapu and those represented by grey dots for lower Bandelier tuff (B), Pozzolan Rosse (P), Rattlesnake tuff (Ra) and Kidnappers (Ki) are not considered in our analysis (see text for explanation).

For concentrated PDCs, Roche et al. (2021) found that the runout distance is

$$R_c = 55 \times 10^{-4} Q^{0.373} \quad (3)$$

The exponent in this power law relationship is significantly smaller than that in Eq. (1) for dilute PDCs. Assuming that the power law relationships that include the particle settling velocity for both dilute (Eq. 2) and concentrated currents have the same exponent, which is unknown a priori, the authors deduced from penalized regression methods that the runout of concentrated PDCs is

$$R_c = 17 \times 10^{-4} (Q/w_c)^{0.456} \quad (4)$$

with  $w_c$  the calculated particle settling velocity equal to  $\sim 1$ -10 m/s and which increases with runout distance. The exponent in Eq. (4) is close to that in Eq. (2) and the theoretical value of 0.5 for dilute currents.

In principle, the PDC travel distance increases during the waxing phase of an eruption while successive flow pulses form units separated by depositional isochrons (Branney and Kokelaar 2002). The leading edge of the current reaches the runout distance at the maximum discharge rate and it eventually moves backward during the waning phase (Fig. 3a) (Williams et al. 2014; Scarpati et al. 2020). The runout of both dilute and concentrated PDCs increases also with the volume of the parent eruptions, which can be explained as the volume correlates positively with the eruption rate (Giordano and Cas 2021, Roche et al. 2021). Therefore, at a given eruption rate that sets the flow runout, larger volumes of erupted material result in greater thicknesses and higher aspect-ratios of PDC deposits as flow units stack up (Fig. 3b). Note that the runout of dilute PDCs also depends on the initial temperature of the mixture (Andrews and Manga 2012).

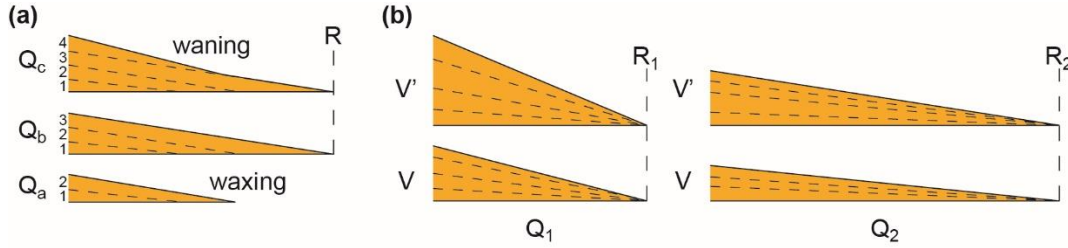


**Fig. 3.** Schematic cross-sections of PDC deposits, with dashed lines representing interfaces of stacked flow units. (a) The distance travelled by a current increases with the discharge rate ( $Q_a$ ) during the waxing phase, the maximum discharge rate ( $Q_b$ ) sets the runout distance ( $R$ ), and the travel distance decreases during the waning phase ( $Q_c < Q_b$ ). Flow units 1 to 4 are shown. (b) Runout as function of hypothetical constant eruption discharge rates ( $Q_1 < Q_2$ ), which control runout distances ( $R_1 < R_2$ ), and eruption volumes ( $V < V'$ ), which control deposit thicknesses.

In this study, we address the fact that the exponent in Eq. (3) is significantly less than 0.5. In fact, concentrated PDCs are channelized in topographic lows. Therefore, at given eruption rate, a channelized current has a longer runout than a current that propagates radially. In this regard, Roche et al. (2022) showed that large-volume caldera-forming eruptions ( $> \sim 500 \text{ km}^3 \text{ DRE}$ ) with mass discharge rates  $> 10^{10} \text{ kg/s}$  can generate PDCs with runouts greater than 300 km when the flows travel in large regional valleys. Here, we discuss PDCs produced by smaller magnitude eruptions with mass discharge rates  $< 10^9 \text{ kg/s}$ , which propagate in valleys of volcanic edifices in proximal areas and over distances typically  $< 20 \text{ km}$ , and for which we recalculate the runout distance assuming radial propagation as discussed below.

To conduct our analysis, we use a slightly revised version of the database of Roche et al. (2021), taking into account that uncertainties exist for a few cases of concentrated PDCs, as discussed by Roche et al. (2022). The revised database is available at <https://doi.org/10.25519/Z1KW-N075>. We consider for the Peach Spring tuff a mean runout distance calculated from measurements in four sub-perpendicular directions. More importantly, we neglect the data for four eruptions, namely the lower Bandelier, Kidnappers, Pozzolane Rosse (also called Tuscalano Artemisio) and Rattlesnake ignimbrites, because their mass discharge rates are determined from models of turbulent dilute current (Bursik and Woods 1991; Dade 2003; Calabrò et al. 2022) while the parent PDCs are interpreted by authors of the original studies as being dominantly concentrated. For the sake of consistency, we prefer not to take these data into account. Furthermore, the runout for these cases is poorly constrained, except for the lower Bandelier tuff (Cook et al. 2016). For instance, for the Pozzolane Rosse ignimbrite a mean runout of 24 km from the topographic boundary of the caldera (and a corresponding mass discharge rate of  $2.7 \times 10^{10} \text{ kg/s}$  according to Fig. 6 of Calabrò et al. 2022) is probably a minimum estimate because the parent currents were strongly affected by orthogonal mountain ridges to the east and they reached the coastline to the west. With these modifications, the runout of concentrated PDCs is (dashed red line in Fig. 2)

$$R_c = 72 \times 10^{-4} Q^{0.358}, \quad (5)$$

which is very close to Eq. (3) given by Roche et al. (2021) for the original data set. This may be explained by the small number of excluded cases compared with the 24 remaining data defining the power-law relationship. We emphasize that the power law relationship including the data from the four neglected large volume eruptions discussed above is  $R_c = 71 \times 10^{-4} Q^{0.359}$  and almost identical to Eq. (5).

### 3. Further analysis for concentrated currents

#### 3.1. Recalculated runout distances

Characteristics of deposits of concentrated PDCs in the database of Roche et al. (2021), with  $Q < 10^9 \text{ kg/s}$  and  $R_c < 20 \text{ km}$  and which propagated partly (e.g., Mount St-Helens; Brand et al. 2014) or entirely (e.g., Soufrière Hills; Druitt et al. 2002) from the vents in valleys of volcanic edifices, are given in Table 1. All concentrated PDCs are channelized, but we distinguish here between the currents mentioned above and currents with long runouts, typical of caldera-forming eruptions, whose propagation is moderately controlled by regional topography and whose deposits are subcircular in map view. For the cases of strong topographic control, we recalculate runouts following Walker et al. (1980) and Giordano and Cas (2021). We measured with Image J<sup>®</sup> (Schneider et al. 2012) the areas of the PDC deposits represented in published maps, then we defined circles of equivalent areas and centered on the vents, and we considered the radii of these circles to be equivalent runouts over unconfined topography (Fig. 4). Note that this method was not applied to the 1992 Spurr eruption, because the deposits area can hardly be determined from the map of Miller et al. (1995), and channeling of some PDCs at Vesuvius cannot be excluded (Gurioli et al. 2010). Table 1 shows that the recalculated runouts are on average  $0.37 \pm 0.19$  times the observed runouts.

The data for the concentrated PDCs including the recalculated runouts discussed above and shown in Fig. 2 give  $R_c = 2.1 \times 10^{-4} Q^{0.507}$ . Note that the data point for Quizapu is outside the 99% prediction interval (possibly due to different physics from other concentrated currents as assumed for this study or incomplete mapping of the deposits described by Hildreth and Drake, 1992) and it was not taken into account for our analysis. The choice of a 99% prediction interval itself reflects a conservative approach, aiming to include as much of the data as possible within the bounds of ‘expected’ behaviour according to the model. Observations falling outside this range are extremely rare under the model's assumptions, reinforcing the argument that the Quizapu case is fundamentally different or not adequately represented by the available data. Consequently, the power law relationship including recalculated runout distances in Fig. 2 is almost identical to the one given above and is equal to

$$R_c = 2.2 \times 10^{-4} Q^{0.508} \quad (6)$$

A notable outcome is that the exponent in Eq. (6) is very close to 0.5, as for dilute currents characterized by axisymmetrical propagation.

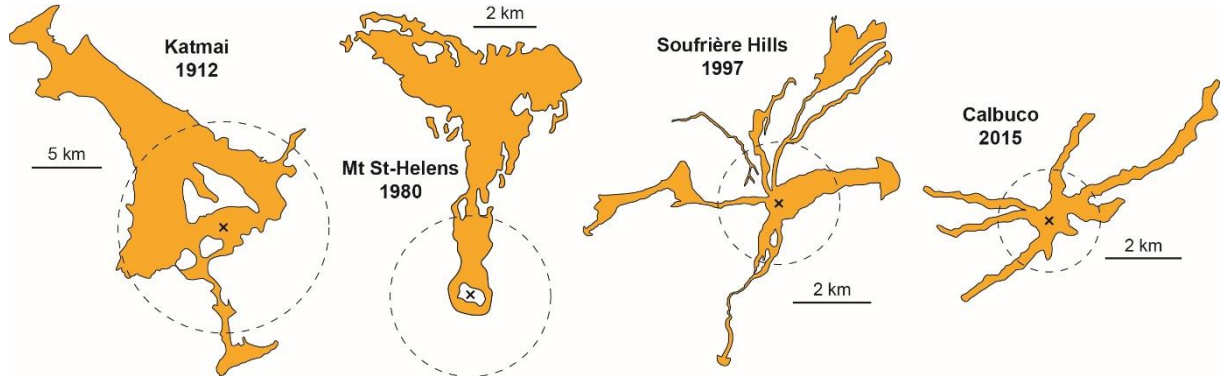


**Fig. 4.** Simplified maps of deposits of channelized concentrated PDCs. Dashed circles have areas equivalent to that of the deposits and are centered on vents indicated by crosses, and respective radii correspond to recalculated runout distances. The maps were redrawn from Fierstein and Hildreth (1992) for Katmai, Brand et al. (2014) for Mount St-Helens, Druitt et al. (2002) for Soufrière Hills, and Castruccio et al. (2016) for Calbuco.

**Table 1.** Characteristics of deposits of channelized PDCs.

Eruption	Age, date	Mean runout (km)	Recalculated runout (km)	Area (km <sup>2</sup> )	Volume <sup>a</sup> (km <sup>3</sup> )	Reference
Calbuco	AD 2015	6	1.3	5.65	0.015	Castruccio et al. (2016)
El Chichon (B-F2)	04/04/1982	5.8	2.0	12.5	0.0077	Macías et al. (1997)
Katmai	AD 1912	19	7.6	180	11	Fierstein and Hildreth (1992)
Kelud	13/02/2014	4.9	1.1	3.85	0.014	Maeno et al. (2019)
Mt St-Helens (IV)	18/05/1980	7.8	2.6	20.6	0.14	Brand et al. (2014)
Pinatubo	15/06/1991	14.5	7.8	193	5.5	Scott et al. (1996)
Quizapu	10-11/04/1932	8.6	1.6	7.6	0.01	Hildreth and Drake (1992)
Reventador	03/11/2002	6.5	2.0	12.5	0.05	Samaniego et al. (2008)
Soufrière Hills	Aug-Oct 1995	3.5	1.6	7.6	0.00037 <sup>b</sup>	Druitt et al. (2002)

<sup>a</sup>Bulk Volume. <sup>b</sup>Average volume of individual PDCs.

### 3.2. Estimation of particle settling velocity in concentrated PDCs

We now estimate particle settling velocity in concentrated PDCs from two different methods and discuss implications for power law relationships that characterize the runout of the currents. For each natural case, we consider a typical settling velocity corresponding to an average particle size and that accounts for the runout of the polydisperse mixture. This is an important limitation of our study which must be taken into account when interpreting the results presented below.

#### 3.2.1. Regression-selection statistical model

We follow the same approach as Roche et al. (2021) and assess the regression optimization problem to estimate both model parameters and missing data of particle settling velocities for concentrated currents,  $w_c$ . However, we consider recalculated runout distances of PDCs as discussed above. We assume that the power law

relationships for both concentrated and dilute currents have a common exponent that is unknown a priori. For the concentrated PDCs, the log-scale data are given by

$$\log(R_c) = \alpha \log\left(\frac{Q_c}{w_c}\right) + \mu_c + \varepsilon \quad (7)$$

where  $\alpha$  and  $\mu_c$  are the slope (i.e. exponent) and the intercept of the regression line, respectively, and  $\varepsilon$  is an unknown error. Note that the line intercept  $\mu_c$  is not necessarily the same as for dilute PDCs,  $\mu_d$ . The missing data  $\alpha$ ,  $\mu_d$ ,  $\mu_c$  and  $w_c$  are obtained by minimizing a penalized cost-function

$$C_{(\alpha, \mu_{d,c}, w_c)} = \sum_{i=1}^n \left\{ \log(R_{d,c}) - \alpha \log\left(\frac{Q_{d,c}}{w_{d,c}}\right) - \mu_{d,c} \right\}^2 + Pen(\alpha, \mu_{d,c}, w_c) \quad (8)$$

where  $R_{d,c}$  and  $Q_{d,c}$  are for a given eruption the known runout and mass eruption rate for a dilute or concentrated current, and  $w_d$  is the known particle settling velocity for a dilute current. Penalization  $Pen(\alpha, \mu_{d,c}, w_c)$  is used to avoid overfitting when there are too many predictors or too few observations. We considered that the power law exponents were either free parameters or that they were equal to the theoretical value of 0.5 for dilute currents, and we found that both approaches yielded very close results. Below we discuss only the case of free exponents.

The typical particle settling velocities in concentrated PDCs we obtain through the regression model are  $\sim 2$ -10 m/s (Table 2). These estimates permit us to determine that the runout of concentrated currents is characterized by

$$R_c = 3.6 \times 10^{-4} (Q/w_c)^{0.528} \quad (9)$$

which is close to the power law relationship for dilute PDCs given by Eq. (2) (Fig. 5).

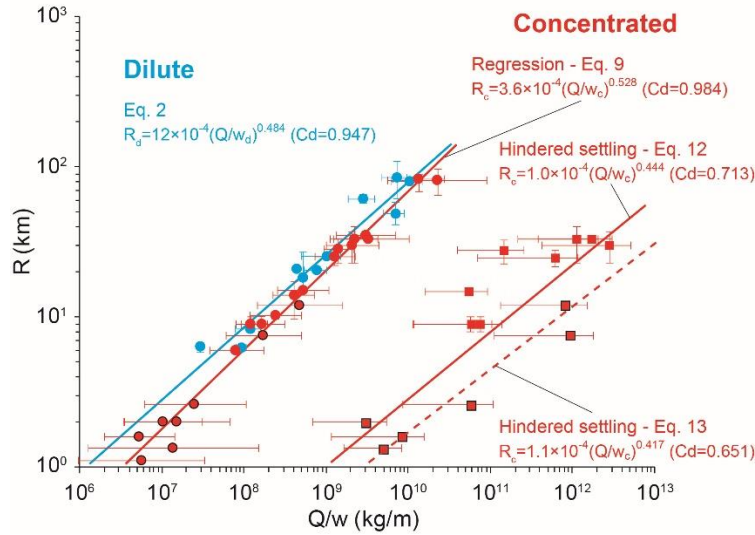


**Fig. 5.** Runout distance of PDCs as function of mass discharge rate,  $Q$ , over particle settling velocity,  $w$ . For concentrated currents (red) the particle settling velocity is that obtained from penalized regression method (circles) or hindered settling model (squares) and it is considered to determine power law relationships given by Eq. (9) and Eqs. (12-13), respectively.  $Cd$  stands for coefficient of determination. Data calculated from hindered settling model are shown for current particle concentration  $\phi_c=0.4$  (Eq. 12). The dashed red line corresponds to Eq. (13) for  $\phi_c=0.5$  (data points are not shown for clarity). Symbols with black contours stand for recalculated runout distances as discussed in the main text.

### 3.2.2. Hindered settling model

Concentrated non-sheared suspensions of particles in a less dense fluid are known to undergo hindered settling, meaning that the particle settling velocity decreases as the solid concentration increases because of enhanced drag of the interstitial fluid moving upwards as a consequence of the downward motion of particles. Hindered settling is widely studied in engineering and was examined by Druitt (1995) and Girolami et al. (2010) in the context of PDCs. Here we assume that the hindered settling model for monodisperse suspensions is suitable to determine the settling velocity of particles in a polydisperse flowing mixture with internal shear. We calculate hindered settling velocities from the empirical relation of Richardson and Zaki (1954) for monodisperse granular suspensions,

$$w_c = w_t(1 - \phi_c)^n \quad (10)$$

where  $w_t$  is the terminal settling velocity of an individual particle in an infinite fluid (here estimated from the method of Rhodes, 2008),  $\phi_c$  is the particle concentration in the suspension, and  $n$  depends on the particle Reynolds number,  $Re_p$ , so that  $n=4.65$  at  $Re_p < 0.2$  while  $n=4.346 \times Re_p^{-0.096}$  at  $Re_p > 0.2$  according to Table 6 of Richardson and Zaki (1954). Note that  $n$  varies very little with the particle shape. In order to assess the suitability of the hindered

settling model, we consider data of experiments of Girolami et al. (2010) on analogue PDCs with ignimbritic material at various particle concentrations. The particle settling velocity could not be measured in these experiments, but it can be inferred from the deposit aggradation rate determined from video analysis. Theoretically, the upper surface of the deposit migrates upwards at velocity

$$U_c = w_c \frac{\phi_c}{(\phi_d - \phi_c)} \quad (11)$$

with  $\phi_d$  the particle concentration in the deposit (Guazelli and Morris 2012, chapter 6.6). We calculated aggradation rates from Eqs. (10-11) by considering two characteristic particle sizes for the ignimbritic material: the mean grain size (Inman parameter) and the Sauter diameter (see Breard et al. 2019 for relevance to PDCs). Fig. 6 shows that the theoretical aggradation velocity increases with the particle concentration as observed in experiments (conversely, the particle settling velocity decreases at increasing concentration). The velocity calculated with the Sauter diameter is much closer to the experimental data, although about twice as small, than in the case where the mean grain size is considered.

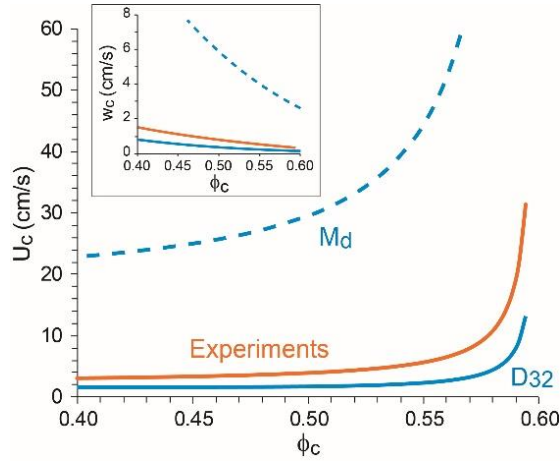


**Fig. 6.** Deposit aggradation velocity,  $U_c$ , calculated from Eqs. (10-11) and observed in experiments of Girolami et al. (2010) as a function of flow particle concentration,  $\phi_c$ . In experiments,  $U_c = [2.44(\phi_d/\phi_c) - 2.15] / [(\phi_d/\phi_c) - 1]$ , with  $\phi_d$  the particle concentration of the deposit assumed to be equal to 0.6. In order to calculate the hindered settling velocity  $w_c$  from Eq. (10) and shown in inset, we consider two characteristic sizes of particles of the experimental material (ash) whose average density is  $1807 \text{ kg/m}^3$ : the mean grain size  $M_d = 144 \text{ }\mu\text{m}$  ( $w_t = 0.72 \text{ m/s}$ ,  $Re_p = 6.9$ , and  $n = 3.61$ ) and the Sauter diameter  $D_{32} = 40 \text{ }\mu\text{m}$  ( $w_t = 0.087 \text{ m/s}$ ,  $Re_p = 0.2$ , and  $n = 4.65$ ), with  $w_t$  and  $Re_p$  calculated from the method of Rhodes (1998) and  $n$  given by Richardson and Zaki (1954).

The above analysis suggests that the hindered settling model for monodisperse non-sheared suspensions predicts reasonably well the particle settling velocity in concentrated polydisperse flows provided the Sauter diameter is taken into account. Accordingly, we have estimated particle settling velocities in concentrated PDCs by considering published grain size data summarized in the database of Roche et al. (2021). For this purpose, we neglected the  $\sim 2$ -fold difference between model results and experimental data shown in Fig. 6 because it is negligible for the power law relationships we discuss hereafter in view of uncertainties about PDCs particle concentrations and grain sizes. When the latter are available in literature, they are given either for one outcrop (whose granulometry does not necessarily reflect that of the erupted material) or at several locations, often at different distances from the vent, and the question then arises of the representative size to be taken into account for the calculations. In the present case, we considered for a given eruption an average value of the published grain sizes. In general, the authors give only mean grain sizes ( $M_d$ ). However, it is possible to infer Sauter diameters ( $D_{32}$ ) when detailed grain size data are available (e.g., Sigurdson and Carey 1989; Burgisser 2005; Breard et al. 2016) and in this regard we could determine that the Sauter diameter is about 3 to 8 times smaller than the mean grain size. Taking into account that  $M_d/D_{32} = 3-8$ , we calculated mean Sauter diameters for PDCs, which are typically in the range  $50-500 \text{ }\mu\text{m}$  (Table 2). These Sauter diameters then enabled us to calculate hindered settling velocities from Eqs. (10-11). Assuming PDCs with particle concentrations of 0.4-0.5, the hindered settling velocities are  $\sim 0.1-10 \text{ cm/s}$  (Table 2). These velocities permitted us to determine that the runout of concentrated currents is characterized by

$$R_c = 1.0 \times 10^{-4} (Q/w_c)^{0.444} \quad (12)$$

$$R_c = 1.1 \times 10^{-4} (Q/w_c)^{0.417} \quad (13)$$

for  $\phi_c = 0.4$  and  $0.5$ , respectively (Fig. 5). These power law relationships are similar to that defined for dilute PDCs but their exponents are less close to the theoretical value 0.5, their prefactors are an order of magnitude smaller, and the data defining them are more scattered due to greater variability in estimated particle settling velocities.

## 4. Discussion

### 4.1. Power law relationships

In order to discuss the power law relationships we present above, we revisit the work of Dade and Huppert (1995) on axisymmetric dilute currents with constant volume flow rate or constant volume. The constant volume flow rate is (Eq. 22 in Dade and Huppert 1995)

$$Q' = 2\pi r h u \quad (14)$$

with  $r$  the distance travelled from the origin, and  $h$  and  $u$  the current height and current speed at  $r$ , respectively. Considering the runout distance  $R_Q$ , the current mean speed is  $u_R = R_Q/t_s$ , with  $t_s = h_R/w$  the particle settling time where  $h_R$  is the current mean height and  $w$  is the particle settling velocity. Eq. (14) can be rewritten as  $Q' = 2\pi R_Q h_R u_R$  so that

$$R_{Q'} = \left( \frac{Q'}{2\pi w} \right)^{0.5} \quad (15)$$

Note that if the current is unidirectional, a similar analysis shows that  $R_{Q'}$  scales with  $Q'/w$ . Therefore, it appears that the exponent 0.5 in Eq. (15) expresses essentially radial propagation of the current.

In case of a current with constant volume  $V$ , the runout distance is (Eq. 7 in Dade and Huppert 1995)

$$R_V = c_1 \left( \frac{g' V^3}{w^2} \right)^{1/8} \quad (16)$$

with  $c_1 \sim 1.1-1.2$  a constant that depends on the Froude number and  $g' = (\rho_p - \rho_i)/\rho_a$  the reduced gravity with  $\rho_p$ ,  $\rho_i$  and  $\rho_a$  the density of the particles, of the interstitial fluid and of the ambient medium, respectively. Let's consider  $V = Q_m' t_c$ , with  $Q_m'$  the mean volume flow rate and  $t_c$  the time of current emplacement given by Eq. (11) of Dade and Huppert (1995),

$$t_c = c_2 \left( \frac{V}{g' w^2} \right)^{1/4} \quad (17)$$

with  $c_2$  a constant  $\sim 1$ , and which is equal to

$$t_c = c_2 \left( \frac{Q_m'}{g' w^2} \right)^{1/3} \quad (18)$$

Eq. (16) can be rewritten

$$R_V = c_1 \left\{ g' \left[ Q_m' c_2 \left( \frac{Q_m'}{g' w^2} \right)^{1/3} \right]^3 / w^2 \right\}^{1/8} \quad (19)$$

which simplifies to

$$R_V = c_1 c_2^{1/8} \left( \frac{Q_m'}{w} \right)^{0.5} \quad (20)$$

with  $c_1 c_2^{1/8} \sim c_1$ .

The above analysis shows that, whatever the initial conditions (constant flow rate or constant volume), the runout of axisymmetric dilute currents varies with the ratio of the flow rate over the particle settling velocity to the power 0.5, the latter being the consequence of radial propagation of the currents.

### 4.2. Internal dynamics of concentrated currents

We now discuss the particle settling velocities in concentrated PDCs we obtained from the regression method or the hindered settling model and which differ by two to three orders of magnitude. Assuming particle concentrations of 0.4-0.5 and 0.6 in PDCs and in their deposits, respectively, the settling velocities of  $\sim 200-1000$  cm/s (regression method) and  $\sim 0.1-10$  cm/s (hindered settling model) given in Table 2 correspond to aggradation velocities of  $\sim 400-5000$  cm/s and  $\sim 0.2-50$  cm/s, respectively. These estimates of aggradation velocities are conservative due to uncertainties about particle sizes and concentrations, in particular.

The aggradation velocities obtained from the hindered settling model are consistent with the data from ash flow experiments by Girolami et al. (2010), as discussed above, and by Breard et al. (2016, with  $U_c = 45-55$  cm/s and  $\phi_c = 0.45-0.50$ ). They are also of the same order as the estimates of Pollock et al. (2019) from analysis of structure of PDC deposits at Mount St-Helens ( $U_c = 4-32$  cm/s). This suggests that the hindered settling model yields realistic particle settling velocities for concentrated PDCs. The fact that the hindered settling velocities we calculated are about two times smaller than those of Girolami et al. (2010) may be due to the polydispersity of the ignimbritic material, the full effects of which are probably not taken into account by the Sauter diameter (another possible cause is internal shear, which favors particle interactions and interstitial fluid motion, but these phenomena are more likely to delay particle fall). This discrepancy, however, is negligible for the power law relationships given by Eqs. (12-13), which suggest that the emplacement of concentrated PDCs obey the same principle as dilute ones. We acknowledge that the difference in the exponents of these relationships from the theoretical value of 0.5 may be significant and may have various causes, in particular more complex physics than those presented in Fig. 1 as well as uncertainties on recalculated runout distances and on estimates of typical

particle settling velocities for the polydisperse mixtures. It appears that the regression method fails in predicting reliable estimates of particle settling velocities, contrary to what Roche et al. (2021) proposed. It is essential to note that the parameters estimated for the unobserved settling velocities in concentrated currents are derived from observed covariates and data from dilute currents. This methodology inherently introduces a bias associated with the different settling mechanisms in both types of flows. To address this limitation, it may be necessary to make additional assumptions based on the fundamental physics. However, this adjustment could compromise the data-driven characteristic of the approach, which ideally should rely exclusively on observed data to accurately model the phenomena. Although the statistical approach does not yield relevant results in the case we have studied, we believe it may be useful in other volcanic contexts and that it is worth presenting the principles here.

Deposit aggradation velocities of  $\sim 0.2\text{-}50$  cm/s discussed above give, for concentrated PDCs of typical thicknesses of 1-10 m, timescales of deposition of the order of a second to an hour. The long timescales are similar to those of emplacement of some PDCs and suggest early onset of deposition. In this case, possible variations in chemical composition in magmatic systems cause temporal fluctuation in the composition of currents emitted at vents, and deposit aggradation leads to vertical compositional zonation in deposits. (Carrasco-Núñez and Branney 2005; Williams et al. 2014). Short time scales, on the other hand, suggest that deposition does not occur for a significant duration of PDC propagation. Pollock et al. (2019) concluded on stepwise aggradation, likely caused by successive events of deposition, non-deposition and possibly erosion as supported by field observation (Brown and Branney 2004) and analogue experiments (Rowley et al. 2011; Chédeville and Roche 2015). Another possible explanation is that PDCs first slide on and erode their substrate as shown by many field examples (e.g., Buesch 1992; Allen and Cas 1998; Brown et al. 2003; LaBerge et al. 2006; Pittari et al. 2007; Brand et al. 2016). In this case, onset of particle deposition occurs at late stages of emplacement once flow velocity and basal shear have decreased below a given threshold which is unknown yet.

## 5. Conclusion

Our simple analysis shows that, assuming axisymmetric propagation, the runout of concentrated PDCs varies with the discharge rate to the power  $\sim 0.5$  as for dilute currents. Although this power law relationship may seem surprising, because of the many uncertainties about the flow mechanisms and the approximations we made to recalculate the runout of concentrated channelized PDCs, it is supported by the analysis of Dade and Huppert (1995) which shows that the power 0.5 has a geometric origin due to the radial propagation of the currents. It appears that the runout of PDCs of fundamentally different natures and governed by complex physics can be described to first order in relatively simple terms and depends primarily on the discharge rate (cf. Bursik and Woods, 1996; Shimizu et al. 2019; Giordano and Cas, 2021; Roche et al. 2021; Calabrò et al. 2022). In this regard, the power law relationships and their prediction intervals defined from natural data represent simple tools that can be used to estimate mass discharge rates of eruptions during the PDC phase from observed runout distances. These relationships are similar to those relating plume height to discharge rate during the initial pre-collapse phase (e.g., Mastin et al. 2009).

The particle settling velocity controls the runout of PDCs to second order. One possible explanation is that the range of the settling velocities is small compared to that of the discharge rates. For concentrated PDCs, we argue that the hindered settling model defined for monodisperse suspensions in a static fluid is relevant for estimating the particle settling velocity provided the Sauter diameter of the polydisperse mixture is taken into account. In this regard, settling velocities are  $\sim 0.1\text{-}10$  cm/s, and corresponding aggradation rates of same order indicate timescales of deposition that are close to or significantly shorter than typical durations of PDCs propagation. Short timescales suggest either stepwise aggradation (Pollock et al. 2019) or that onset of particle deposition occurs at late stage of emplacement. The latter is consistent with the fact that concentrated PDCs often erode the substrate on which they propagate.

## Acknowledgments

We thank Associate Editor Michael Ort, Guido Giordano and an anonymous reviewer for their constructive comments. This is ClerVolc contribution n° 653.

## Declarations

Competing Interests. The authors declare no competing interests.

**Table 2.** Particle settling velocities in concentrated PDCs determined from statistical or particle hindered settling models.

Eruption	Age, date	Particle settling velocity, $w_c$ (cm/s)		Mean runout, R (km) <sup>c</sup>	Mass discharge rate, Q (kg/s) <sup>c</sup>	Reference
		Statistical model <sup>a</sup>	Hindered settling <sup>b</sup>			
Bishop tuff	0.765 Ma	<b>515</b> (245-1085)	<b>0.9</b> (0.4-1.4)	30	$1.1 \times 10^{10}$	<a href="#">Hildreth and Mahood (1986)</a>
Calbuco	AD 2015		<b>9.0</b> (4.8-13.2)	6	$3.7 \times 10^8$	<a href="#">Castruccio et al. (2016)</a>
Cerro Blanco	4.2 ka	<b>578</b> (250-1338)		35	$1.8 \times 10^{10}$	<a href="#">Fernandez-Turiel et al. (2019)</a>
Crater Lake	5783±49 BP	<b>810</b> (266-2469)		33	$2.7 \times 10^{10}$	<a href="#">Bacon (1983)</a>
El Chichón (B-F2)	04/04/1982		<b>2.6</b> (1.3-4.0)	5.8	$5.0 \times 10^7$	<a href="#">Macias et al. (1997)</a>
Ilopango (unit F)	270-735 AD	<b>435</b> (235-807)	<b>1.7</b> (0.8-2.7)	33	$1.0 \times 10^{10}$	<a href="#">Pedrazzi et al. (2019)</a>
Katmai	AD 1912		<b>0.3</b> (0.1-0.5)	19	$1.2 \times 10^9$	<a href="#">Fierstein and Hildreth (1992)</a>
Kos (unit E)	161.3 ka	<b>331</b> (217-505)	<b>4.7</b> (2.4-7.0)	28	$4.7 \times 10^9$	<a href="#">Allen et al. (1999)</a>
Ksudach	240 AD	<b>400</b> (222-720)		14	$1.7 \times 10^9$	<a href="#">Braitseva et al. (1996)</a>
Mount St. Helens (IV)	18/05/1980		<b>0.9</b> (0.4-1.4)	7.8	$2.2 \times 10^8$	<a href="#">Brand et al. (2016)</a>
Okmok II	2050 BP	<b>486</b> (235-1003)	<b>11.6</b> (6.4-16.9)	15	$2.6 \times 10^9$	<a href="#">Burgisser (2005)</a>
Peach Spring tuff	18.8 Ma	<b>1056</b> (268-4165)		81	$2.4 \times 10^{11}$	<a href="#">Buesch (1992)</a>
Pinatubo	15/06/1991		<b>1.1</b> (0.5-1.7)	14.5	$4.1 \times 10^9$	<a href="#">Scott et al. (1996)</a>
Quizapu	10-11/04/1932		<b>1.5</b> (0.7-2.3)	8.6	$2.0 \times 10^9$	<a href="#">Hildreth and Drake (1992)</a>
Soufrière Hills	19/06/1995		<b>0.5</b> (0.2-0.8)	3.5	$1.7 \times 10^7$	<a href="#">Cole et al. (2002)</a>
Tambora	1815 AD	<b>410</b> (232-725)	<b>2.7</b> (1.3-4.1)	25	$5.3 \times 10^9$	<a href="#">Self et al. (1984)</a>
Tungurahua	1916 AD	<b>461</b> (222-952)		10.3	$1.1 \times 10^9$	<a href="#">Hall et al. (1999)</a>
Toba (Young tuff)	75 ka	<b>438</b> (213-999)		82	$5.9 \times 10^{10}$	<a href="#">Aldiss and Ghazali (1984)</a>
Vesuvius (Pomici di base)	18.3-22.5 ka	<b>417</b> (195-887)		6	$3.4 \times 10^8$	<a href="#">Gurioli et al. (2010)</a>
Vesuvius (Pollena)	472 AD	<b>226</b> (146-1349)	<b>0.8</b> (0.4-1.3)	9	$2.8 \times 10^8$	<a href="#">Gurioli et al. (2010)</a>
Vesuvius	1631 AD	<b>381</b> (204-708)	<b>2.0</b> (1.0-3.1)	9	$6.5 \times 10^8$	<a href="#">Gurioli et al. (2010)</a>

<sup>a</sup> Minimum and maximum estimates in brackets from 95 % uncertainty intervals.

<sup>b</sup> Mean values of estimates given in brackets and calculated for mean particle [Sauter](#) diameters 3 to 8 times smaller than the mean grain sizes and assuming particle concentrations of 0.4 to 0.5.

<sup>c</sup> See [Roche et al. \(2021\)](#) for details.

## References

- Aldiss DT, Ghazali SA (1984) The regional geology and evolution of the Toba volcano-tectonic depression, Indonesia. *J Geol Soc London* 141:487-500, doi:410.1144/gsjgs.1141.1143.0487.
- Allen SR, Cas RAF (1998) Lateral variations within coarse co-ignimbrite lithic breccias of the Kos Plateau Tuff, Greece. *Bull Volcanol* 59:356-377.
- Allen SR, Stadlbauer E, Keller J (1999) Stratigraphy of the Kos Plateau Tuff: product of a major Quaternary explosive rhyolitic eruption in the eastern Aegean, Greece. *Int J Earth Sci* 88:132-156.
- Andrews B, Manga M (2012) Experimental study of turbulence, sedimentation, and coignimbrite mass partitioning in dilute pyroclastic density currents. *J Volcanol Geotherm Res* 225-226:30-44, doi: 10.1016/j.jvolgeores.2012.1002.1011.
- Andrews BJ (2014) Dispersal and air entrainment in unconfined dilute pyroclastic density currents. *Bull Volcanol* 76:852, doi: 810.1007/s00445-00014-00852-00444.
- Aravena A, Cioni R, Bevilacqua A, de' Michieli Vitturi M, Esposti Ongaro T, Neri A (2020) Tree-branching-based enhancement of kinetic energy models for reproducing channelization processes of pyroclastic density currents. *J Geophys Res: Solid Earth* 125:e2019JB019271.
- Bacon C (1983) Eruptive history of Mount Mazama and Crater Lake caldera, Cascade range, USA. *J Volcanol Geotherm* 18:57-115.
- Benage MC, Dufek J, Mothes PA (2016) Quantifying entrainment in pyroclastic density currents from the Tungurahua eruption, Ecuador: Integrating field proxies with numerical simulations. *Geophys Res Lett* (43):6932-6941, doi: 6910.1002/2016GL069527.
- Bevilacqua A, Aravena A, Aspinall W, Costa A, Mahony S, Neri A, Sparks S, Hill B (2022) Assessing minimum pyroclastic density current mass to impact critical infrastructures: example from Aso caldera (Japan). *Nat Hazards Earth Syst Sci* 22:3329-3348.
- Braitseva OA, Melekestsev IV, Ponomareva VV, Kirianov VY (1996) The caldera-forming eruption of Ksudach volcano about Cal. A.D. 240: the greatest explosive event of our era in Kamchatka, Russia. *J Volcanol Geotherm Research* 70:49-65.
- Brand BD, Bendaña S, Self S, Pollock N (2016) Topographic controls on pyroclastic density current dynamics: Insight from 18 May 1980 deposits at Mount St. Helens, Washington (USA). *J Volcanol Geotherm* 321:1-17, <http://dx.doi.org/10.1016/j.jvolgeores.2016.1004.1018>.
- Brand BD, Mackaman-Lofland C, Pollock NM, Bendaña S, Dawson B, Wichgers P (2014) Dynamics of pyroclastic density currents: Conditions that promote substrate erosion and self-channelization - Mount St Helens, Washington (USA). *J Volcanol Geotherm* 276:189-214, <http://dx.doi.org/110.1016/j.jvolgeores.2014.1001.1007>.
- Brandt L, Coletti F (2022) Particle-laden turbulence: progress and perspectives. *Ann Rev Fluid Mech* 54:159-189
- Branney MJ, Kokelaar BP (2002) Pyroclastic density currents and the sedimentation of ignimbrites. *Geol Soc London, Memoirs* 27.
- Breard ECP, Lube G, Jones JR, Dufek J, Cronin SJ, Valentine GA, Moebis A (2016) Coupling of turbulent and non-turbulent flow regimes within pyroclastic density currents. *Nature Geosci* 9:767-771, doi: 710.1038/NGEO2794.
- Breard ECP, Jones J, Fullard L, Lube G, Davies C, Dufek J (2019) The Permeability of Volcanic Mixtures - Implications for Pyroclastic Currents. *Journal of Geophysical Research: Solid Earth* 124:1343-1360, <https://doi.org/1310.1029/2018JB016544>.
- Brosch E, Lube G (2020) Spatiotemporal sediment transport and deposition processes in experimental dilute pyroclastic density currents. *J Volcanol Geotherm* 401:106946.
- Brown RJ, Barry TL, Branney MJ, Pringle MS, Bryan SE (2003) The Quaternary pyroclastic succession of southeast Tenerife, Canary Islands: explosive eruptions, related caldera subsidence, and sector collapse. *Geol Mag* 140(3):265-288, doi: 210.1017/S0016756802007252.
- Brown RJ, Branney MJ (2004) Bypassing and diachronous deposition from density currents: evidence from a giant regressive bed form in the Poris ignimbrite, Tenerife, Canary Islands. *Geology* 35(5):445-448, doi: 410.1130/G20188.20181.
- Buesch DC (1992) Incorporation and redistribution of locally derived lithic fragments within a pyroclastic flow. *Geol Soc Am Bull* 104:1193-1207.
- Burgisser A (2005) Physical volcanology of the 2,050 BP caldera-forming eruption of Okmok volcano, Alaska. *Bull Volcanol* 67:497-525.
- Bursik MI, Woods AW (1996) The dynamics and thermodynamics of large ash-flows. *Bulletin of Volcanology* 58:175-193.
- Calabró L, Esposti Ongaro T, Giordano G, de' Michieli Vitturi M (2022) Reconstructing pyroclastic currents' source and flow parameters from deposit characteristics and numerical modeling: The Pozzolane Rosse ignimbrite case study (Colli Albani, Italy). *J Geophys Res: Solid Earth* 127:e2021JB023637.
- Carrasco-Núñez G, Branney MJ (2005) Progressive assembly of a massive layer of ignimbrite with normal-to-reverse compositional zoning: the Zaragoza ignimbrite of central Mexico. *Bull Volcanol* 68:3-20, doi 10.1007/s00445-005-0416-8.
- Carazzo G, Kaminski E, Tait S (2008) On the dynamics of volcanic columns: a comparison of field data with a new model of negatively buoyant jets. *J Volcanol Geotherm Res* 178:94-103, doi: 110.1016/j.volgeores.2008.1001.1002.
- Castruccio A, Clavero J, Segura A, Samaniego P, Roche O, Le Pennec J-L, Drogue B (2016) Eruptive parameters and dynamics of the April 2015 sub-Plinian eruptions of Calbuco volcano (southern Chile). *Bull Volcanol* 78:62, doi: 10.1007/s00445-00016-01058-00448.
- Charbonnier SJ, Germa A, Connor CB, Gertisser R, Preece K, Komorowski J-C, Lavigne F, Dixon T, Connor L (2013) Evaluation of the impact of the 2010 pyroclastic density currents at Merapi volcano from high-resolution satellite imagery, field investigations and numerical simulations. *J Volcanol Geotherm* 261:295-315.
- Charbonnier SJ, Garin F, Rodríguez LA, Ayala K, Cancel S, Escobar-Wolf R, Chigna G, Chun-Quinillo C, González D, Chigna W, Chun-Quinillo K, Mérida R, Juárez F, Calder HS (2023) Unravelling the dynamics and hazards of the June 3rd, 2018,

- pyroclastic density currents at Fuego volcano (Guatemala). *J Volcanol Geotherm* 436:107791, <https://doi.org/10.1016/j.jvolgeores.2023.107791>.
- Chédeville C., O. Roche (2015). Influence of slope angle on pore pressure generation and kinematics of pyroclastic flows: Insights from laboratory experiments. *Bull Volcanol* 77: 96, doi: 10.1007/s00445-015-0981-4.
- Chen C, Dai Q, Qi H (2016) Improvement of EMMS drag model for heterogeneous gas–solid flows based on cluster modeling. *Chem Eng Sci* 141:8–16, <http://dx.doi.org/10.1016/j.ces.2015.1010.1025>.
- Cole PD, Calder ES, Sparks RSJ, Clarke AB, Druitt TH, Young SR, Herd RA, Harford CL, Norton GE (2002) Deposits from dome-collapse and fountain-collapse pyroclastic flows at Soufrière Hills Volcano, Montserrat. In: Druitt TH, Kokelaar BP (eds) *The eruption of Soufrière Hills Volcano, Montserrat, from 1995-1999*. Geological Society, London, pp 231-262.
- Cook GW, Wolff JA, Self S (2016) Estimating the eruptive volume of a large pyroclastic body: the Otowi Member of the Bandelier Tuff, Valles caldera, New Mexico. *Bull Volcanol* 78:10, doi: 10.1007/s00445-00016-01000-00440.
- Dade WD (2003) The emplacement of low-aspect ratio ignimbrites by turbulent parent flows. *Journal of Geophysical Research* 108(B4): 2211. Dade WB, Huppert HH (1995) Runout and fine-sediment deposits of axisymmetric turbidity currents. *J Geophys Res* 100(c9):18597-18609.
- Delanney R, Valance A, Mangeney A, Roche O, Richard P (2017) Granular and particle-laden flows: from laboratory experiments to field observations, *J Phys D: Applied Physics* 50, 053001, doi: 10.1088/1361-6463/50/5/053001.
- Dellino P, Dioguardi F, Rinaldi A, Sulpizio R, Mele D (2021) Inverting sediment bedforms for evaluating the hazard of dilute pyroclastic density currents in the field. *Sci Reports* 11:21024.
- Dellino P, Mele D, Sulpizio R, La Volpe L, Braia G (2008) A method for the calculation of the impact parameters of dilute pyroclastic density currents based on deposit particle characteristics. *J Geophys Res* 113:B07206, doi: 10.1029/2007JB005365.
- de' Michieli Vitturi M, Esposti Ongaro T, Lari G, Aravena A (2019) IMEX\_SfloW2D 1.0: a depth-averaged numerical flow model for pyroclastic avalanches. *Geoscientific Model Development* 12:581-595, <https://doi.org/10.5194/gmd-12-581-2019>.
- Doronzo DM, Dellino P (2013) Hydraulics of subaqueous ash flows as deduced from their deposits: 2. Water entrainment, sedimentation, and deposition, with implications on pyroclastic density current deposit emplacement. *J Volcanol Geotherm* 258:176-186.
- Douillet GA, Pacheco DA, Kueppers U, Letort J, Tsang-Hin-Sun E, Bustillos J, Hall M, Ramón P, Dingwell DB (2013) Dune bedforms produced by dilute pyroclastic density currents from the August 2006 eruption of Tungurahua volcano, Ecuador. *Bull Volcanol* 75: 762, doi: 10.1007/s00445-00013-00762-x.
- Doyle EE, Hogg AJ, Mader HM (2011) A two-layer approach to modelling transformation of dilute pyroclastic currents into dense pyroclastic flows. *Proc Roy Soc A* 467:1348-1371, doi: 10.1098/rspa.2010.0402.
- Druitt TH (1995) Settling behaviour of concentrated dispersions and some volcanological applications. *J Volcanol Geotherm Res* 65:27-39.
- Druitt TH (1998) Pyroclastic density currents. In: Gilbert JS, Sparks RSJ (eds) *The physics of explosive volcanic eruptions*. Geol Soc London Spec Pub, pp 145-182.
- Druitt TH, Calder ES, Cole PD, Hoblitt RP, Loughlin SC, Norton GE, Ritchie LJ, Sparks RSJ, Voight B (2002) Small-volume, highly mobile pyroclastic flows formed by rapid sedimentation from pyroclastic surges at Soufrière Hills Volcano, Montserrat: an important volcanic hazard. In: Druitt TH, Kokelaar BP (eds) *The eruption of Soufrière Hills Volcano, from 1995 to 1999*. Geol Soc London, Memoirs, pp 263-279.
- Dufek J (2016) The fluid mechanics of pyroclastic density currents. *Ann Rev Fluid Mech* 48:459-485, doi: 10.1146/annurev-fluid-122414-034252.
- Dufek J, Bergantz GW (2007) Suspended load and bed-load transport of particle-laden gravity currents: the role of particle-bed interaction. *Theoretical Computational Fluid Dynamics* 21:119-145, doi: 10.1007/s00162-007-0041-6.
- Esposti Ongaro T, Komorowski J-C, Legendre Y, Neri A (2020) Modelling pyroclastic density currents from a subplinian eruption at La Soufrière de Guadeloupe (West Indies, France). *Bull Volcanol* 82:76. <https://doi.org/10.1007/s00445-020-01411-6>.
- Fauria KE, Manga M, Chamberlain M (2016) Effect of particle entrainment on the runout of pyroclastic density currents. *J Geophys Res: Solid Earth* 121:6445–6461, doi: 10.1002/2016JB013263.
- Fernandez-Turiel JL, Perez-Torrado FJ, Rodriguez-Gonzalez A, Saavedra J, Carracedo JC, Rejas M, Lobo A, Osterrieth M, Carrizo JI, Esteban G, Gallardo J, Ratto N (2019) The large eruption 4.2 ka cal BP in Cerro Blanco, Central Volcanic Zone, Andes: Insights to the Holocene eruptive deposits in the southern Puna and adjacent regions. *Estudios Geológicos* 75(1):e088, <https://doi.org/10.3989/egeol.43438.43515>.
- Fierstein J, Hildreth W (1992) The plinian eruptions of 1912 at Novarupta, Katmai National Park, Alaska. *Bull Volcanol* 54:646-684.
- Fisher RV (1979) Models for pyroclastic surges and pyroclastic flows. *J Volcanol Geotherm* 6:305-318.
- Giordano G, Cas RAF (2021) Classification of ignimbrites and their eruptions. *Earth Sci Rev* 220:103697.
- Giordano G, Dobran F (1994) Computer simulation of the Tuscalano Artemisio's second pyroclastic flow unit (Alban hills, Latium, Italy). *Journal of Volcanology and Geothermal Research* 61:69-94.
- Girolami L, Roche O, Druitt TH, Corpetti T (2010) Velocity fields and depositional processes in laboratory ash flows. *Bull Volcanol*, 72: 747–759, doi: 10.1007/s00445-010-0356-9.
- Guazzelli E, Morris J (2012) *A physical introduction to suspension dynamics*. Cambridge University Press, pp. 229.
- Gueugneau V, Charbonnier SJ, Esposti Ongaro T, de' Michieli Vitturi M, Peruzzetto M, Mangeney A, Bouchut F, Patra A, Kelfoun K (2021) Synthetic benchmarking of concentrated pyroclastic current models. *Bull Volcanol* 83:75.
- Gurioli L, Sulpizio R, Cioni R, Sbrana A, Santacroce R, Luperini W, Andronico A (2010) Pyroclastic flow hazard assessment at Somma–Vesuvius based on the geological record. *Bulletin of Volcanology* 72:1021-1038, doi: 10.1007/s00445-00010-00379-00442.

- Gustavsson K, Mehlig B (2016) Statistical models for spatial patterns of heavy particles in turbulence. *Adv Physics* 65(1):1-57.
- Hall ML, Robin C, Beate B, Mothes P, Monzier C (1999) Tungurahua Volcano, Ecuador: structure, eruptive history and hazards. *J Volcanol Geotherm* 91:1-21.
- Hildreth W, Drake RE (1992) Volcan Quizapu, Chilean Andes. *Bull Volcanol* 54:93-125.
- Hildreth W, Mahood GA (1986) Ring fracture eruption of the Bishop tuff. *Geol Soc Am Bull* 97:396-403.
- Kelfoun K (2017) A two-layer depth-averaged model for both the dilute and the concentrated parts of pyroclastic currents, *J Geophys Res: Solid Earth*, 122, 4293-4311, doi: 10.1002/2017JB014013.
- Kelfoun K, Samaniego P, Palacios P, Barba D (2009) Testing the suitability of frictional behaviour for pyroclastic flow simulation by comparison with a well-constrained eruption at Tungurahua volcano (Ecuador). *Bull Volcanol* 71:1057-1075, doi: 10.1007/s00445-00009-00286-00446.
- LaBerge R, Giordano G, Cas RAF, Ailleres L (2006) Syn-depositional substrate deformation produced by the shear force of a pyroclastic density current: An example from the Pleistocene ignimbrite at Monte Cimino, northern Lazio, Italy. *J Volcanol Geotherm Res* 158: 307-320.
- Lube G, Breard ECP, Jones J, Fullard L, Dufek J, Cronin SJ, Wang T (2019) Generation of air lubrication within pyroclastic density currents. *Nature Geosci* 12:381-386, <https://doi.org/310.1038/s41561-41019-40338-41562>.
- Lube G, Breard ECP, Esposti-Ongaro T, Dufek J, Brand B (2020) Multiphase flow behaviour and hazard prediction of pyroclastic density currents. *Nature Rev Earth Env* 1:348-365.
- Macías JL, Sheridan MF, Espíndola JM (1997) Reappraisal of the 1982 eruptions of El Chichón Volcano, Chiapas, Mexico: new data from proximal deposits. *Bull Volcanol* 58:459-471.
- Maeno F, Nakada S, Yoshimoto M, Shimano T, Hokanishi N, Zaennudin A, Iguchi M (2019) A sequence of a plinian eruption preceded by dome destruction at Kelud volcano, Indonesia, on February 13, 2014, revealed from tephra fallout and pyroclastic density current deposits. *J Volcanol Geotherm Res* 382:24-41, <http://dx.doi.org/10.1016/j.jvolgeores.2017.1003.1002>.
- Mastin LG, Guffanti M, Servranckx R, Webley P, Barsotti S, Dean K, Durant A, Ewert JW, Neri A, Rose WI, Schneider D, Siebert L, Stunder B, Swanson G, Tupper A, Volentik A, Waythomas CF (2009) A multidisciplinary effort to assign realistic source parameters to models of volcanic ash-cloud transport and dispersion during eruptions. *J Volcanol Geotherm Res* 186:10-21, doi:10.1016/j.jvolgeores.2009.1001.1008.
- Miller TP, Neal CA, Waitt RB (1995) Pyroclastic flows of the 1992 Crater Peak eruptions: distribution and origin. *US Geol Sur Bull* 2139:81-87.
- Ogburn SE, Calder ES (2017) The relative effectiveness of empirical and physical models for simulating the dense undercurrent of pyroclastic flows under different emplacement conditions. *Frontiers Earth Sci* 5:83, doi: 10.3389/feart.2017.00083.
- Ort MH (1993) Eruptive processes and caldera formation in a nested downsag collapse caldera: Cerro Panizos, central Andes Mountains. *J Volcanol Geotherm Res* 56:221-252.
- Ort MH, Orsi G, Pappalardo L, Fisher RV (2003) Anisotropy of magnetic susceptibility studies of depositional processes in the Campanian Ignimbrite, Italy. *Bull Volcanol* 65: 55–72. <https://doi.org/10.1007/s00445-002-0241-2>.
- Pedrazzi D, Sunye-Puchol I, Aguirre-Díaz G, Costa A, Smith VC, Poret M, Dávila-Harris P, Miggins DP, Hernández W, Gutiérrez E (2019) The Ilopango Tierra Blanca Joven (TBJ) eruption, El Salvador: Volcano-stratigraphy and physical characterization of the major Holocene event of Central America. *J Volcanol Geotherm* 377:81-102.
- Penlou B, Roche O, Manga M, van den Wildenberg S (2023a) Experimental measurement of enhanced and hindered particle settling in turbulent gas-particle suspensions, and geophysical implications. *J Geophys Res: Solid Earth*, 128, e2022JB025809. <https://doi.org/10.1029/2022JB025809>.
- Penlou B., Roche O., van den Wildenberg S. (2023b). Experimental study of the generation of pore gas pressure in pyroclastic density currents resulting from eruptive fountain collapse. *J Geophys Res: Solid Earth*, 128, e2023JB027510. <https://doi.org/10.1029/2023JB027510>.
- Pimentel A, Self S, Pacheco JM, Jeffery AJ, Gertisser R (2021) Eruption style, emplacement dynamics and geometry of peralkaline ignimbrites: insights from the Lajes-Angra ignimbrite formation, Terceira Island, Azores. *Frontiers Earth Sci* 9: 673686.
- Pittari A, Cas RAF, Monaghan JJ, Martí J (2007) Instantaneous dynamic pressure effects on the behaviour of lithic boulders in pyroclastic flows: the Abrigo Ignimbrite, Tenerife, Canary Island. *Bull Volcanol* 69:265-279, doi: 210.1007/s00445-00006-00072-00447.
- Pollock N, Brand BD, Rowley PJ, Sarocchi D, Sulpizio R (2019) Inferring pyroclastic density current flow conditions using syn-depositional sedimentary structures. *Bull Volcanol* 81:46, <https://doi.org/10.1007/s00445-00019-01303-z>.
- Rhodes MJ (1998) Introduction to Particle Technology. John Wiley and Sons, Chichester, pp 315.
- Richardson JF, Zaki WN (1954) Sedimentation and fluidisation: Part I. *Trans Instn Chem Engrs* 32:S82-100.
- Roche O, Montserrat S, Niño Y, Tamburrino A (2010) Pore fluid pressure and internal kinematics of gravitational laboratory air-particle flows: insights into the emplacement dynamics of pyroclastic flows. *J Geophys Res: Solid Earth*, 115, B09206, doi: 10.1029/2009JB007133.
- Roche O, Azzaoui N, Guillin A (2021) Discharge rate of explosive volcanic eruption controls runout distance of pyroclastic density currents. *Earth Planet Sci Lett* 568:117017.
- Roche O, Henry C, Azzaoui N, Guillin A (2022) Long-runout pyroclastic density currents: analysis and implications. *Geology*, 50: 1172–1176. <https://doi.org/10.1130/G50215.1>.
- Rowley PJ, Kokelaar BP, Menzies M, Waltham D (2011) Shear-derived mixing in dense granular flows. *J Sedim Res* 81:974-884, doi: 910.2110/jsr.2011.2172.
- Samaniego P, Eissen J-P, Le Pennec J-L, Robin C, Hall ML, Mothes P, Chavrit D, Cotten J (2008) Pre-eruptive physical conditions of El Reventador volcano (Ecuador) inferred from the petrology of the 2002 and 2004–05 eruptions. *J Volcanol Geotherm* 176:82-93, doi:10.1016/j.jvolgeores.2008.1003.1004.

- Scarpati C, Sparice D, Perrotta A (2020) Dynamics of large pyroclastic currents inferred by the internal architecture of the Campanian Ignimbrite. *Sci Rep* 10: 22230. <https://doi.org/10.1038/s41598-020-79164-7>.
- Schneider, C.A., Rasband, W.S., Eliceiri, K.W., 2012. NIH Image to ImageJ: 25 years of image analysis. *Nat Methods* 9, 671-675. doi:10.1038/nmeth.2089.
- Scott WE, Hoblitt RP, Torres RC, Self S, Martinez MML, Nillos TJ (1996) Pyroclastic flows of the June 15, 1991, climactic eruption of mount Pinatubo. In: Newhall CJ, Punongbayan RS (eds) *Fire and Mud: eruptions and lahars of mount Pinatubo, Philippines*. Philippine Institute of Volcanology and Seismology, University of Washington Press, Quezon city, Seattle and London, pp 545-570.
- Self S, Rampino MR, Newton MS, Wolff JA (1984) Volcanological study of the great Tambora eruption of 1815. *Geology* 12:659-663.
- Shimizu HA, Koyaguchi T, Suzuki YJ (2019) The run-out distance of large-scale pyroclastic density currents: A two-layer depth-averaged model. *J Volcanol Geotherm Res* 381:168-184, <https://doi.org/10.1016/j.jvolgeores.2019.1003.1013>.
- Shimizu HA, Koyaguchi T, Suzuki YJ (2023) Dynamics and deposits of pyroclastic density currents in magmatic and phreatomagmatic eruptions revealed by a two-layer depth-averaged model. *Geophysical Research Letters* 50:e2023GL104616.
- Sigurdsson H, Carey S (1989) Plinian and co-ignimbrite tephra fall from the 1815 eruption of Tambora volcano. *Bulletin of Volcanology* 51:243-270.
- Sulpizio R, Castioni D, Rodriguez-Sedano LA, Sarocchi D, Lucchi F (2016) The influence of slope-angle ratio on the dynamics of granular flows: insights from laboratory experiments. *Bull Volcanol* 78:77, doi: 10.1007/s00445-00016-01069-00445.
- Sweeney MR, Valentine GA (2017) Impact zone dynamics of dilute mono- and polydisperse jets and their implications for the initial conditions of pyroclastic density currents. *Phys Fluids* 29:093304, doi: 093310.091063/093301.5004197.
- Tadini A, Bevilacqua A, Neri A, Cioni R, Biagioli G, de'Michieli Vitturi M, Esposti Ongaro T (2021) Reproducing pyroclastic density current deposits of the 79 CE eruption of the Somma–Vesuvius volcano using the box-model approach. *Solid Earth* 12:119-139.
- Trinh T, Boltenhagen P, Delannay R, Valance A (2017) Erosion and deposition processes in surface granular flows. *Phys Rev E* 96:042904, doi: 042910.041103/PhysRevE.042996.042904.
- Valentine GA (1987) Stratified flow in pyroclastic surges. *Bull Volcanol* 49:616-630.
- Valentine GA (2020) Initiation of dilute and concentrated pyroclastic currents from collapsing mixtures and origin of their proximal deposits. *Bull Volcanol* 82:20, <https://doi.org/10.1007/s00445-00020-01366-x>.
- Walker GPL, Heming RF, Wilson CJN (1980) Low-aspect ratio ignimbrites. *Nature* 283: 286-287.
- Williams R, Branney MJ, Barry TL (2014) Temporal and spatial evolution of a waxing then waning catastrophic density current revealed by chemical mapping. *Geology* 42(2):107-110, doi: 10.1130/G34830.1.